Suppression of Coercivity in Nanoscale Graded Magnetic Materials

Lorenzo Fallarino,[1] Mikel Quintana,[1] Eva López Rojo,[1,2] and Andreas Berger[1]

[1] *CIC nanoGUNE BRTA, E-20018 Donostia - San Sebastián, Spain*

[2] *Faculty of Science, University of Valladolid, E-47011 Valladolid, Spain*

(Received 17 June 2021; accepted 6 August 2021; published 22 September 2021)

We investigate temperature-dependent magnetization reversal of CoRu graded films, in which a predefined depth-dependent exchange-coupling strength J follows a V-shaped profile. Magnetometry reveals an extended temperature range below the Curie temperature T_C where the reversal of the magnetization M is not accompanied by the conventionally occurring hysteresis, in stark contrast with homogeneous CoRu reference films. This is caused by the temperature-driven paramagnetic (PM)-ferromagnetic (FM) phase transition, which does not occur in the entirety of the graded material but only in well-defined nanoscopic regions at any given temperature, enabling the creation of two internal PM/FM interfaces that assist the external magnetic field in reversing the magnetization of the FM graded sample region. Hysteretic reversal is recovered at sufficiently low sample temperatures or by using graded structures with very steep J gradients, so that no PM/FM interfaces form inside the exchange-coupled layer material that could influence the magnetization reversal process. Our findings open interesting material design options, and we envision wide application potential, since we succeed in engineering a temperature gap between the temperature dependent magnetization and hysteresis onsets, a capability of interest for any technology benefitting from field-free magnetization switching.

DOI: 10.1103/PhysRevApplied.16.034038

The continuous demands of technologies for advancing specific aspects of magnetic materials properties to overcome technical challenges have made magnetization reversal a core area of active research during the last several decades [1–6]. The fundamental process corresponds to the change in magnetization (M) direction caused by applying an opposite magnetic field (H) [7] and can occur via domain formation [8,9], or magnetization rotation or switching [10]. The latter process is generally associated with a discontinuous jump in the corresponding $M(H)$ curve, which is related to the first order phase transition that ferromagnets undergo below their Curie temperature (T_C) upon magnetic field inversion. Owing to the existence of multiple energy minima, which can be populated within a temperature-dependent magnetic field range, such magnetization reversal is typically hysteretic. The width of the hysteresis along the magnetic field axis, whose upper limit is set by the anisotropy field H_K, is most commonly characterized by coercive fields $H_C < H_K$ [11], determines the utility and application range of magnetic materials. Its manipulation has now become an important challenge in order to make major technological progress.

In this regard, the magnetocaloric effect (MCE), which is of great interest for disruptive solid-state-based refrigeration technology, is one particular application where the proper tuning of hysteresis properties is crucial. In fact, MCE materials are typically used near T_C, but the developing hysteresis below T_C leads to problems in terms of data evaluation, as well as the overall magnetocaloric performance and efficient energy conversion due to energy losses [6,12]. Hard disk drives are another example where hysteresis tuning is of substantial relevance. In fact, the growing importance of increasing the areal bit density has encouraged considerable efforts to manipulate H_C by using electric fields [13,14], by ferromagnetic (FM) resonance [15–17], by temporarily heating the media during the recording process [18,19], or by using spin-polarized currents [20–25].

Although a high level of refinement has been achieved, researchers have yet to find pathways to expand the range of accessible strategies to manipulate the hysteresis characteristics by further adapting materials' properties [26]. In this respect, exchange-spring ferromagnets have been demonstrated to be an interesting material type. They are formed from soft and hard magnetic layers that are ferromagnetically exchange coupled at their interface [27–29]. Here, the strong susceptibility (χ) of the soft material enhances the external field effect on the whole exchange-coupled structure, promoting χ as an additional means to manipulate and control hysteretic behavior. In this regard, it is worthwhile to realize that the paramagnetic (PM) states of ferromagnets exhibit properties of purely PM materials, in particular the linear dependence of the magnetization with an applied field. Intriguingly, in the vicinity of T_C, they exhibit extremely high χ values, much larger than in pure paramagnets due to the still active ordering force. Therefore, if appropriately coupled, the PM states of ferromagnets should be able to greatly influence the magnetization reversal of adjacent ferromagnets with higher T_C.

Recently, works on rationally designed exchange-coupling profiled samples have demonstrated that although ferromagnetism is a long-range collective phenomenon, the local magnetic properties of graded magnetic materials are dominated by the corresponding local material properties down to distances of a few nanometers [30–35]. Even at this scale, they behave almost as if they are composed of virtually independent layers, each with its own "local" Curie temperature ($\hat{T}_C$). However, from a thermodynamic perspective, such an exchange-coupled system does not truly exhibit multiple phase transitions, but instead only one, with a "global" Curie temperature $T_C = \hat{T}_C^{\max}$. Therefore, exchange graded structures allow the creation of materials that are ferromagnetically coupled throughout and at the same time have a certain section of the sample that is always at the respective $\hat{T}_C$ (locally acquiring very high χ values) within a designed temperature window. Thus, the main motivation of this work is to investigate whether and how exchange graded materials can actually impact and specifically reduce coercivities in a relevant temperature range below T_C. This would offer interesting material design options that could be important for multiple technical applications pursuing low-field or field-free magnetization switching [36–41].

In this Letter, we consider the temperature-dependent magnetization reversal properties of V-shaped CoRu graded samples. To generate reliable results, in which only a depth dependence of the magnetization occurs, our graded magnetic films are grown epitaxially, following the specific layer sequence shown in Fig. 1(a) [10,42–44]. Underlayers of (110) Ag and (211) Cr are deposited on the Si substrates to promote highly oriented (211) $Cr_{0.71}Ru_{0.29}$ layers, which in turn serve as a template for the epitaxial growth of a (10$\bar{1}$0) $Co_{1-x(z)}Ru_{x(z)}$ compositionally graded layer. The samples are finally capped with a 10-nm-thick protective SiO_2 layer. By linearly varying the Ru content, from $x_{\min} = 0.325$ at the center to $x_{\max} = 0.37$ at the bottom and top, we achieve a depth-dependent exchange-coupling strength J (and thus $\hat{T}_C$) that is described by

$$J(z) = J_0\,(1 - s|z|), \tag{1}$$

with J_0 ($\hat{T}_C^{\max}$) being the maximum value in the center ($z = 0$). The slope $s > 0$ is defined as $(1 - \hat{T}_C^{\min}/\hat{T}_C^{\max})/(t/2)$, with $10\,\text{nm} \leq t \leq 150$ nm being the CoRu thickness, and $\hat{T}_C^{\min}$ and $\hat{T}_C^{\max}$ referring to the T_C values of homogenous $Co_{0.63}Ru_{0.37}$ and $Co_{0.675}Ru_{0.325}$ samples [10,44], respectively. It is worthwhile mentioning that $\hat{T}_C^{\min}$ and $\hat{T}_C^{\max}$ in our structures are different from the $\hat{T}_C$ values of our homogenous $Co_{0.63}Ru_{0.37}$ and $Co_{0.675}Ru_{0.325}$ reference samples when t becomes sufficiently small due to the finite-thickness effect [45]. However, given that the thickness dependence of T_C for homogenous films is universal for identical lattice structures and surface orientations, the ratio $\hat{T}_C^{\min}/\hat{T}_C^{\max}$, which is part of the definition of s, should not be greatly affected by varying t. Thus, the quantity s and its values represent a meaningful description of our samples by quantifying the J reduction (as a percentage of J_0) per nanometer [45], and furthermore serve as an indicator of the compositional gradient in our structures that is associated with the corresponding exchange-coupling strength J and relative $\hat{T}_C$ profiles. We explore nine different slopes s of the J profile while keeping $\Delta J = J_0 - J_{\min}$ fixed, with the largest and smallest s samples schematically depicted in Fig. 1(b). Cu $K\alpha$ X-ray diffractometry confirms the epitaxial growth quality, as shown in Fig. 1(c). Well-defined peaks are observed corresponding to Si (220), Ag (220), Cr (211), CrRu (211), and CoRu (10$\bar{1}$0) crystal planes [10,30]. For comparison purposes, homogeneous epitaxial $Co_{0.653}Ru_{0.347}$ samples, having the average Ru content of the graded structures, are fabricated using an identical underlayer sequence.

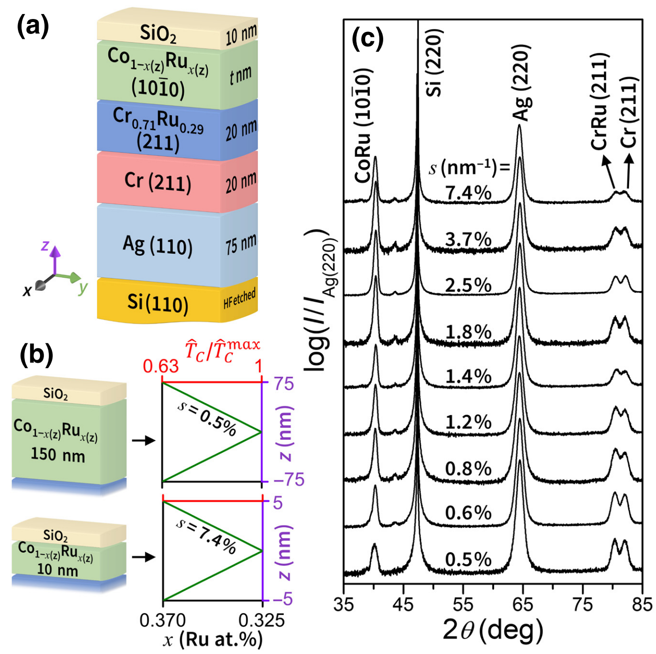

FIG. 1. (a) Schematic of the layer growth sequence. (b) Ru content and the associated effective Curie temperature $\hat{T}_C$ depth profile for the two extreme cases of graded $Co_{1-x(z)}Ru_{x(z)}$ layers 10 nm ($s = 7.4\%$) and 150 nm ($s = 0.5\%$) thick. (c) XRD $\theta/2\theta$ scans for samples with different s. Each scan is normalized to the intensity of its Ag (220) peaks and vertically offset by a constant value to permit comparison.

The temperature-dependent easy-axis magnetization reversal $M(H)$ is measured in steps of 2 K in the temperature range from 80 to 300 K using a superconducting

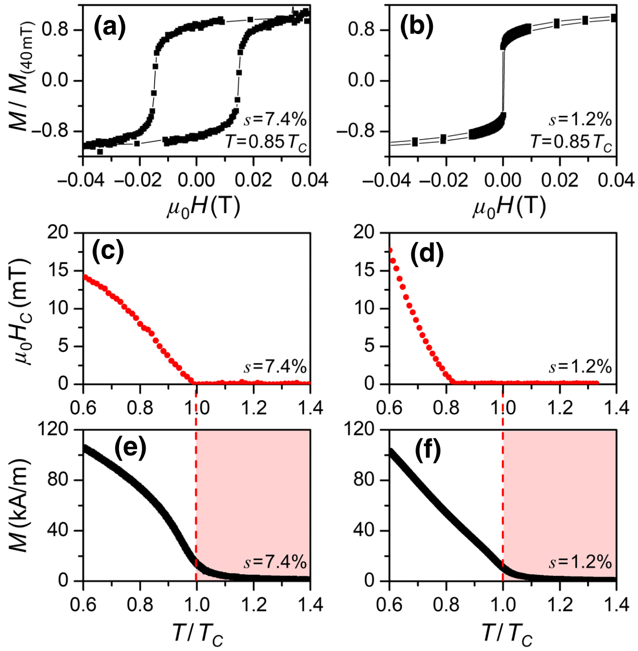

FIG. 2. (a) and (b) $M(H)$ measurements along the easy axes for two different samples with $s = 7.4\%$ (a) and $s = 1.2\%$ (b), both measured at $T/T_C(s) = 0.85$. Here, the M data are normalized to their values at $\mu_0 H = 40$ mT. (c) and (d) coercive field H_C versus temperature for $s = 7.4\%$ (c) and $s = 1.2\%$ (d). (e) and (f) temperature dependence of the magnetization M for samples with $s = 7.4\%$ (e) and $s = 1.2\%$ (f). The $M(T)$ data are measured in the presence of an applied field $\mu_0 H = 4$ mT along the easy magnetization axis.

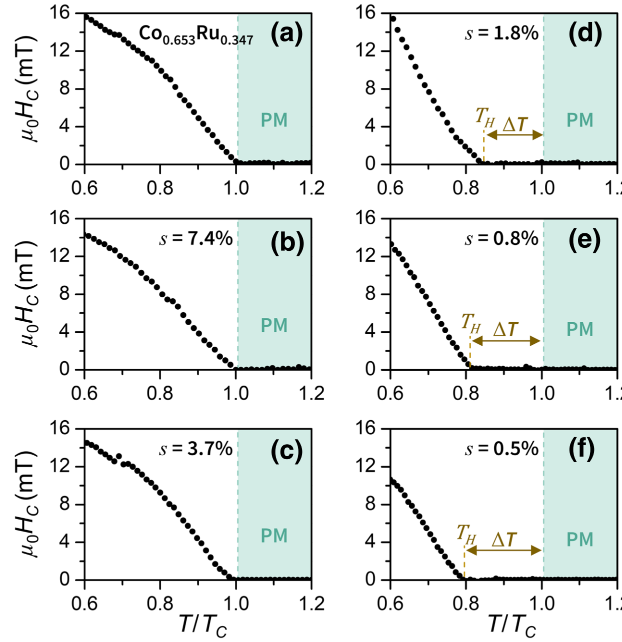

FIG. 3. Temperature dependence of the coercive field $\mu_0 H_C$ for $Co_{0.653}Ru_{0.347}$ homogeneous (a), and graded samples with $s = 7.4\%$ (b), 3.7% (c), 1.8% (d), 0.8% (e), and 0.5% (f). The highlighted light green regions correspond to the temperature range where the samples are paramagnetic, whereas the yellow and green dashed vertical lines in (d)–(f) define the ΔT range of anhysteretic behavior below T_C.

quantum interference device (SQUID) magnetometer. Figures 2(a) and 2(b) show the results for two graded samples with $s = 7.4\%$ (a) and $s = 1.2\%$ (b), both measured at a temperature corresponding to 85% of their global T_C (s). In Fig. 2(a) the data show that the magnetization saturates above a sufficiently high (positive or negative) magnetic field and by decreasing its magnitude to zero, the magnetization shows a remanent value very close to saturation. If the field is further decreased, M is inverted and changes to negative values at a nonzero H_C value. In contrast to this rather conventional behavior, the sample with $s = 1.2\%$ exhibits negligible hysteretic behavior, with the reversal of the magnetization occurring at values of H_C smaller than our experimental resolution of $\mu_0 \Delta H = 0.2$ mT, even though it still shows full saturation and remanent magnetization values. Figures 2(c) and 2(d) display the extracted H_C values as a function of temperature in direct comparison with the $M(T)$ characteristics (measured in the presence of $\mu_0 H = 4$ mT) that are plotted in Figs. 2(e) and 2(f) for graded samples with $s = 7.4\%$ [Figs. 2(c) and 2(e)] and $s = 1.2\%$ [Figs. 2(d) and 2(f)]. For the sample with $s = 7.4\%$ both the onset of FM order and the onset of hysteresis coincide at T_C, marked by the vertical red dashed line, as in any conventional ferromagnet. In contrast, the two onset points for $M(T)$ and $H_C(T)$ are very clearly separated for the $s = 1.2\%$ sample, with the temperature range of virtually field-free magnetization reversal extending far below the sample T_C. These data clearly show that the degree of the continuous depth modification of J has a profound impact on the hysteretic behavior of such nanoscale materials.

Figures 3(a)–3(f) show six exemplary H_C (T) data sets. For a visual comparison, the temperature axes are normalized to each sample's T_C. The resulting temperature dependence of the coercive field for the $Co_{0.653}Ru_{0.347}$ sample, displayed in Fig. 3(a), exhibits the expected sharp coercive field onset at T_C. Similar characteristics are found in the graded structure with $s = 7.4\%$ in Fig. 3(b), and $s = 3.7\%$ in Fig. 3(c), even though both M and J depth profiles are present in these samples, confirming that the resulting magnetic state along the film's depth is strongly correlated, just as it is in a conventional magnetic system. The effect of materials design by means of J grading becomes significant upon decreasing s further, Figs. 3(d)–3(f), where the $H_C(T)$ data show the existence of a temperature gap (ΔT) between T_C and T_H, with the latter temperature defined as the temperature below which a relevant coercivity larger than zero can be measured.

The actual T_C values for our graded samples are shown in Fig. 4(a) as a function of s, together with the T_C

values of $Co_{0.675}Ru_{0.325}$ and $Co_{0.63}Ru_{0.37}$ uniform samples. As expected, the T_C values of our graded structures exhibit a noticeable reduction with thickness in agreement with our previous findings [45], and similar to what has been observed for homogenous films in the past [46]. We determine T_H by fitting the experimental $H_C\,(T)$ data to a power law function multiplied by $\theta(T_H - T)$, which is the Heaviside function. The resulting $\Delta T = (T_C - T_H)$ values, normalized to each sample's T_C, are shown in Fig. 4(b) as a function of s and are very different depending on the specific gradient structure. $\Delta T \approx 0$ for the uniform and high-s value graded samples indicate that the occurrence of FM order and hysteresis are strongly correlated. However, by decreasing s, it is clearly possible to separate the onset of FM order from the hysteresis onset to a relevant degree, namely by at least 18% of the corresponding T_C values. It should be also taken into consideration that in our study ΔJ is constant, and thus a variation of s is always associated with a change in t [44]. Therefore, if one would choose a different ΔJ, the exact numerical ΔT vs s values may change, given that they now correspond to different t values [44]. However, the association of ΔT with s is the most meaningful, because without any gradient structure, the observed behavior would not occur.

In order to properly understand the underlying physics of the evaluated ΔT values, one should consider how the V-shaped graded material orders magnetically close to T_C [30,31,35,42,45,46]. For the case of high s samples, the magnetization along the depth dimension is already largely populated at T_C, as depicted in inset I of Fig. 4, since for such large gradients the total thickness is comparable with the internal magnetic profile width at T_C [30,31,35,42,44–46]. Therefore, even in the presence of a magnetization depth profile, a collective FM behavior develops in the entire film with the absence of PM-like portion that could significantly aid the magnetization reversal, and thus result in a conventional $H_C\,(T)$ behavior. On the contrary, for low s samples, the FM state at T_C forms in the sample's center first, resulting in a magnetization profile whose thickness is considerably smaller than the total material thickness [30,31,35,42,44–46]. This FM region is delimited by two PM regions on its top and bottom, as depicted in inset II of Fig. 4, developing a sort of PM/FM/PM trilayer. At this point, when a magnetic field is applied opposite to the magnetization of the central FM region, the PM regions build up a magnetic moment proportional to their susceptibility χ. Such induced moments die out exponentially with the distance away from the PM/FM interfaces, since χ follows a specific depth profile with its maximum exactly at these interfaces, as depicted in inset II of Fig. 4. This is a consequence of the $\hat{T}_C$ distribution that follows the V-shaped J profile [30,31,35,42,44–46], so that for a range of sample temperatures, the PM/FM interfaces are located at the very position where the local $\hat{T}_C$ is identical to the sample's temperature, and correspondingly χ is maximum

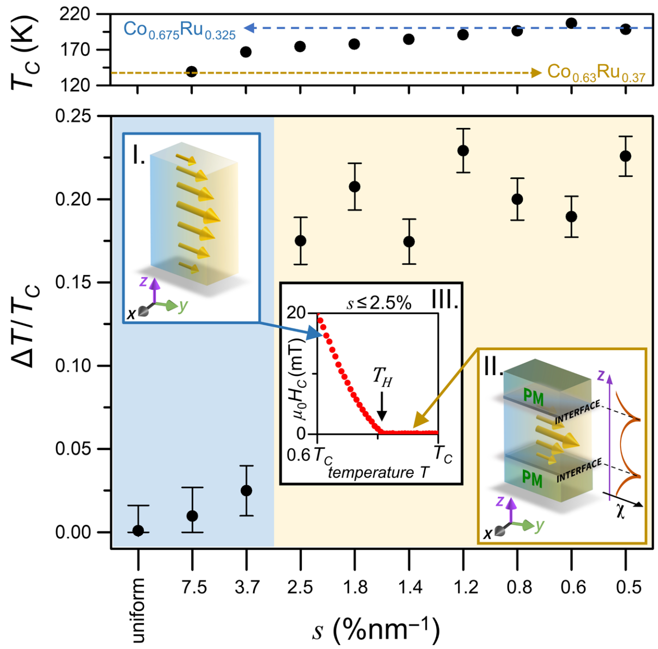

FIG. 4. (a) T_C values of our graded structures as a function of s, together with the T_C values of the $Co_{0.675}Ru_{0.325}$ (blue dashed line) and $Co_{0.63}Ru_{0.37}$ (gold dashed line) uniform samples. (b) s dependence of the $\Delta T/T_C$ temperature range. Inset I schematically shows the magnetization depth profile below T_C for systems with high s values, whereas inset II illustrates the magnetization depth profile with the two characteristic PM sample regions that form below T_C for samples with low s. Inset III displays an exemplar $\mu_0 H_C\,(T)$ for $s \leq 2.5\%$ and the corresponding temperature ranges where the graded samples adopt the magnetization profiles shown in I (low temperature region) and in II (high temperature region).

at that very location (inset II of Fig. 4). In this state, the magnetization of the FM region is antiparallel to the induced PM magnetization upon applying a magnetic field. Thus, this configuration is energetically unfavorable because it increases the FM interlayer exchange energy, which is proportional to the exchange coupling at the PM/FM interface. Consequently, the FM layer reversal is assisted by an interface energy term proportional to the exchange at the PM/FM interfaces that reduces the coercive field, since it favors the parallel alignment of M(PM) and M(FM). As a result, the interface energy term aids magnetization reversal if M(FM) and H are opposite to each other.

Upon lowering the temperature below the global T_C in such samples, the magnetization in the central FM region increases its magnitude and widens its profile, pushing the PM/FM interfaces towards the top and bottom of the graded CoRu material. Thus, upon lowering the temperature, the magnetic profile extends further and further into the film depth dimension. However, for a significant temperature range, its width is smaller than the actual film thickness, so that PM/FM interfaces continue to exist and accordingly H_C stays very small due to the exchange fields at such internal interfaces. Finally, when the sample crosses T_H, as indicated in inset III of Fig. 4, H_C increases as in a conventional ferromagnet. This is because the exchange fields at the PM/FM interfaces have become either negligible or have vanished due to having been moved all the way to the natural material CrRu/CoRu and CoRu/SiO_2 interfaces that lack FM exchange coupling in CrRu or SiO_2. Therefore, by controlling the sample temperature, nonhysteretic magnetization switching can be deterministically promoted or suppressed, and the transition temperature T_H can be designed and controlled by the specifically chosen nanoscale structures.

In summary, graded materials can be harnessed to engineer a gap between the magnetization onset and the hysteresis onset, and this offers broadly applicable technological potential beyond the reach of existing materials technologies. This is due to the interface geometry type phase transition that occurs in materials with a V-shaped exchange-coupling strength profile and that we are able to achieve by properly designing our graded magnetic materials [30,31,35,42,44–46]. Correspondingly, we can disentangle the occurrence of hysteresis from the occurrence of ferromagnetism at T_C, and make ΔT a quantity that can be tuned by altering the nanoscale material characteristics. For large s values the samples behave similarly to homogenous systems, where the occurrence of FM order and hysteresis are strongly correlated at T_C and $\Delta T \approx 0$. In contrast, for sufficiently small s values, the magnetic state has both FM and PM phases present in the same structure for a predesigned temperature range. As a result, such a "mixed" configuration significantly impacts the magnetization reversal behavior, which is driven by the hysteresis-free paramagnetic $M(H)$ relationship of the PM segments, and substantially reduces H_C values smaller than $\mu_0 H = 0.2$ mT within a broad temperature range extending far below T_C. The explored graded structures are designed to be FM below room temperature just to take full advantage of the sensitivity of SQUID measurements, but the physics should apply to any temperature range that may be desired. Finally, our results demonstrate that predefined compositional nanostructure design can be utilized to realize performance advances in any application relying on strong thermomagnetic response in low magnetic fields [13–26]. In addition, similar graded structures have shown high MCE values over a large and tunable temperature range, leading to an improved cooling capacity [47]. Following our experimental results, this approach could thus be utilized to tailor the MCE to achieve major advances in applications such as magnetic refrigeration.

ACKNOWLEDGMENTS

We acknowledge financial support by the Spanish Ministry of Science and Innovation under the Maria de Maeztu Units of Excellence Program (MDM-2016-0618), Project No. RTI2018-094881-B-100 and the Ph.D. Fellowship No. PRE2019-088428.

[1] S. N. Piramanayagam and K. Srinivasan, Recording media research for future hard disk drives, J. Mag. Mag. Mat. **321**, 485 (2009).

[2] D. D. Awschalom, L. C. Bassett, A. S. Dzurak, E. L. Hu, and J. R. Petta, Quantum spintronics: Engineering and manipulating atom-like spins in semiconductors, Science **339**, 1174 (2013).

[3] R. Skomski, Nanomagnetics, J. Phys.: Condens. Matter **15**, R841 (2003).

[4] S. Bader, Colloquium: Opportunities in nanomagnetism, Rev. Mod. Phys. **78**, 1 (2006).

[5] O. Hellwig, A. Berger, J. B. Kortright, and E. E. Fullerton, Domain structure and magnetization reversal of antiferromagnetically coupled perpendicular anisotropy films, J. Mag. Mag. Mat. **319**, 13 (2007).

[6] O. Gutfleisch, M. A. Willard, E. Brück, C. H. Chen, S. G. Sankar, and J. Ping Liu, Magnetic materials and devices for the 21st century: Stronger, lighter, and more energy efficient, Adv. Mater. **23**, 821 (2011).

[7] G. Bertotti, *Hysteresis in Magnetism: for Physicists, Materials Scientists, and Engineers* (Academic Press, San Diego, CA, USA, 1998).

[8] L. Fallarino, O. Hovorka, and A. Berger, Field orientation dependence of magnetization reversal in thin films with perpendicular magnetic anisotropy, Phys. Rev. B **94**, 064408 (2016).

[9] L. Fallarino, A. Oelschlägel, J. A. Arregi, A. Bashkatov, F. Samad, B. Böhm, K. Chesnel, and O. Hellwig, Control of domain structure and magnetization reversal in thick Co/Pt multilayers, Phys. Rev. B **99**, 024431 (2019).

[10] O. Idigoras, U. Palomares, A. K. Suszka, L. Fallarino, and A. Berger, Magnetic properties of room temperature grown epitaxial $Co_{1-x}Ru_x$ alloy films, Appl. Phys. Lett. **103**, 102410 (2013).

[11] D. Givord, M. F. Rossignol, and V. M. T. S. Barthem, The physics of coercivity, J. Magn. Magn. Mater. **258–259**, 1 (2003).

[12] O. Gutfleisch, T. Gottschall, M. Fries, D. Benke, I. Radulov, K. P. Skokov, H. Wende, M. Gruner, M. Acet, P. Entel, and M. Farle, Mastering hysteresis in magnetocaloric materials, Phil. Trans. R. Soc. A **374**, 20150308 (2016).

[13] D. Chiba, M. Yamanouchi, F. Matsukura, and H. Ohno, Electrical manipulation of magnetization reversal in a ferromagnetic semiconductor, Science **301**, 943 (2003).

[14] T. Maruyama, Y. Shiota, T. Nozaki, K. Ohta, N. Toda, M. Mizuguchi, A. A. Tulapurkar, T. Shinjo, M. Shiraishi, S. Mizukami, Y. Ando, and Y. Suzuki, Large voltage-induced magnetic anisotropy change in a few atomic layers of iron, Nature Nanotech. **4**, 158 (2009).

[15] J. G. Zhu, X. Zhu, and Y. Tang, Microwave assisted magnetic recording, IEEE Trans. Magn. **44**, 125 (2007).

[16] H. T. Nembach, P. M. Pimentel, S. J. Hermsdoerfer, B. Leven, B. Hillebrands, and S. O. Demokritov, Microwave

assisted switching in a $Ni_{81}Fe_{19}$ ellipsoid, Appl. Phys. Lett. **90**, 062503 (2007).

[17] T. Yoshioka, T. Nozaki, T. Seki, M. Shiraishi, T. Shinjo, Y. Suzuki, and Y. Uehara, Microwave-assisted magnetization reversal in a perpendicularly magnetized film, Appl. Phys. Exp. **3**, 013002 (2010).

[18] R. E. Rottmayer, S. Batra, D. Buechel, W. A. Challener, J. Hohlfeld, Y. Kubota, L. Li, B. Lu, C. Mihalcea, K. Mountfield, K. Pelhos, C. Peng, T. Rausch, M. A. Seigler, D. Weller, and X.-M. Yang, Heat-assisted magnetic recording, IEEE Trans. Magn. **42**, 2417 (2006).

[19] M. H. Kryder, E. C. Gage, T. W. McDaniel, W. A. Challener, R. E. Rottmayer, G. Ju, Y.-T. Hsia, and M. F. Erden, Heat assisted magnetic recording, Proc. IEEE **96**, 1810 (2008).

[20] J. Slonczewski, Current-driven excitation of magnetic multilayers, J. Magn. Magn. Mater. **159**, L1 (1996).

[21] L. Berger, Emission of spin waves by a magnetic multilayer traversed by a current, Phys. Rev. B **54**, 9353 (1996).

[22] M. Tsoi, A. G. M. Jansen, J. Bass, W.-C. Chiang, M. Seck, V. Tsoi, and P. Wyder, Excitation of a Magnetic Multilayer by an Electric Current, Phys. Rev. Lett. **80**, 4281 (1998).

[23] E. B. Myers, D. C. Ralph, J. A. Katine, R. N. Louie, and R. A. Buhrman, Current-induced switching of domains in magnetic multilayer devices, Science **285**, 867 (1999).

[24] F. J. Albert, J. A. Katine, R. A. Buhrman, and D. C. Ralph, Spin-polarized current switching of a Co thin film nanomagnet, Appl. Phys. Lett. **77**, 3809 (2000).

[25] D. Pinna, A. Mitra, D. L. Stein, and A. D. Kent, Thermally assisted spin-transfer torque magnetization reversal in uniaxial nanomagnets, Appl. Phys. Lett. **101**, 262401 (2012).

[26] T. Gottschall, K. P. Skokov, M. Fries, A. Taubel, I. Radulov, F. Scheibel, D. Benke, S. Riegg, and O. Gutfleisch, The exchange-spring magnet: A new material principle for permanent magnets, Adv. Energy Mat. **9**, 1901322 (2019).

[27] F. Kneller and R. Hawig, The exchange-spring magnet: a new material principle for permanent magnets, IEEE Trans. Magn. **27**, 3588 (1991).

[28] E. Goto, N. Hayashi, T. Miyashita, and K. Nakagawa, Magnetization and switching characteristics of composite thin magnetic films, J. Appl. Phys. **36**, 2951 (1965).

[29] E. E. Fullerton, J. S. Jiang, and S. D. Bader, Hard/soft magnetic heterostructures: Model exchange-spring magnets, J. Magn. Magn. Mater. **200**, 392 (1999).

[30] B. J. Kirby, L. Fallarino, P. Riego, B. B. Maranville, C. W. Miller, and A. Berger, Nanoscale magnetic localization in exchange strength modulated ferromagnets, Phys. Rev. B **98**, 064404 (2018).

[31] B. J. Kirby, H. F. Belliveau, D. D. Belyea, P. A. Kienzle, A. J. Grutter, P. Riego, A. Berger, and C. W. Miller, Spatial Evolution of the Ferromagnetic Phase Transition in an Exchange Graded Film, Phys. Rev. Lett. **116**, 047203 (2016).

[32] C. LeGraët, T. R. Charlton, M. McLaren, M. Loving, S. A. Morley, C. J. Kinane, R. M. D. Brydson, L. H. Lewis, S. Langridge, and C. H. Marrows, Temperature controlled motion of an antiferromagnet-ferromagnet interface within a dopant-graded FeRh epilayer, APL Mater. **3**, 041802 (2015).

[33] M. Marcellini, M. Pärnaste, B. Hjörvarsson, and M. Wolff, Influence of the distribution of the inherent ordering temperature on the ordering in layered magnets, Phys. Rev. B **79**, 144426 (2009).

[34] C. A. Ramos, D. Lederman, A. R. King, and V. Jaccarino, New Antiferromagnetic Insulator Superlattices: Structural and Magnetic Characterization of (FeF2)m(CoF2)n, Phys. Rev. Lett. **65**, 2913 (1990).

[35] L. Fallarino, B. J. Kirby, and E. E. Fullerton, Graded magnetic materials, J. Phys. D: Appl. Phys. **54**, 303002 (2021).

[36] D. Weller, G. Parker, O. Mosendz, E. Champion, B. Stipe, X. Wang, T. Klemmer, G. Ju, and A. Ajan, A HAMR media technology roadmap to an areal density of 4 Tb/in^2, IEEE Trans. Magn. **50**, 1 (2014).

[37] I. L. Prejbeanu, M. Kerekes, R. C. Sousa, H. Sibuet, O. Redon, B. Dieny, and J. P. Nozières, Thermally assisted MRAM, J. Phys.: Condens. Matter **19**, 165218 (2007).

[38] X. Moya, S. Kar-Narayan, and N. D. Mathur, Caloric materials near ferroic phase transitions, Nature Mat. **13**, 439 (2014).

[39] I. M. Miron, K. Garello, G. Gaudin, P.-J. Zermatten, M. V. Costache, S. Auffret, S. Bandiera, B. Rodmacq, A. Schuhl, and P. Gambardella, Perpendicular switching of a single ferromagnetic layer induced by in-plane current injection, Nature **476**, 189 (2011).

[40] L. Rehm, G. Wolf, B. Kardasz, E. Cogulu, Y. Chen, M. Pinarbasi, and A. D. Kent, Thermal Effects in Spin-Torque Switching of Perpendicular Magnetic Tunnel Junctions at Cryogenic Temperatures, Phys. Rev. Appl. **15**, 034088 (2021).

[41] Q. Xie, W. Lin, S. Sarkar, X. Shu, S. Chen, L. Liu, T. Zhao, C. Zhou, H. Wang, J. Zhou, S. Gradečak, and J. Chen, Field-free magnetization switching induced by the unconventional spin–orbit torque from WTe_2, APL Mater. **9**, 051114 (2021).

[42] L. Fallarino, B. J. Kirby, M. Pancaldi, P. Riego, A. L. Balk, C. W. Miller, P. Vavassori, and A. Berger, Magnetic properties of epitaxial CoCr films with depth-dependent exchange-coupling profiles, Phys. Rev. B **95**, 134445 (2017).

[43] M. Quintana, E. Oblak, J. M. Marín Ramírez, and A. Berger, Experimental exploration of the vector nature of the dynamic order parameter near dynamic magnetic phase transitions, Phys. Rev. B **102**, 094436 (2020).

[44] L. Fallarino, E. López Rojo, M. Quintana, B. J. Kirby, and A. Berger, Modifying Critical Exponents of Magnetic Phase Transition via Nanoscale Materials Design, Phys. Rev. Lett. (to be published).

[45] J. S. Salcedo-Gallo, L. Fallarino, J. D. Alzate-Cardona, E. Restrepo-Parra, and A. Berger, Monte carlo simulations of the thermodynamic behavior of exchange graded ferromagnets, Phys. Rev. B **103**, 094440 (2021).

[46] D. Fuchs, T. Schwarz, O. Morán, P. Schweiss, and R. Schneider, Finite-size shift of the curie temperature of ferromagnetic lanthanum cobaltite thin films, Phys. Rev. B **71**, 092406 (2005).

[47] J. S. Salcedo-Gallo, A. Berger, M. Quintana, E. Restrepo-Parra, and L. Fallarino, Nanoscale control of temperature operation ranges for magnetocaloric applications, J. Phys. D: Appl. Phys. **54**, 304003 (2021).